Polymer 51 (2010) 3560–3567

Contents lists available at ScienceDirect

Polymer

journal homepage: www.elsevier.com/locate/polymer

Morphology evolution, crystalline orientation, and thermal expansion of PA6/SEBS blends with nanolayer networks

Guozhang Wu*, Haibo Xu, Ting Zhou

Shanghai Key Laboratory of Advanced Polymeric Materials, School of Materials Science & Engineering, East China University of Science & Technology, Shanghai 200237, PR China

ARTICLE INFO

Article history:
Received 11 January 2010
Received in revised form
10 March 2010
Accepted 28 May 2010
Available online 8 June 2010

Keywords:
Thermal expansion
Polymer alloy
Crystalline orientation

ABSTRACT

A blend of polyamide 6 (PA6) and styrene-ethylene/butylene-styrene (SEBS) with a co-continuous nanolayer network was fabricated by reactive compounding and subsequent injection molding. The nanostructured polymer alloy was found to exhibit an extremely low coefficient of linear thermal expansion (CLTE) in the flow direction, accompanied by a largely suppressed molding shrinkage. To clarify the influence of the microstructure on thermal expansion behavior, a systematic study of morphology evolution, crystalline orientation, and confined crystallization of the PA6/SEBS (60/40) blend was carried out by means of TEM, DMA, DSC and WAXD measurements. It was found that a lower viscosity of SEBS and the capability of *in situ* compatibility with PA6 enable a morphology evolution from a disordered co-continuous to droplet-continuous and, finally, to a nanolayer network structure. Multi-scale orientations take place during the injection molding process, and the large reduction of CLTE may originate from the high order microstructure in two aspects: (1) the rubber-deformation-induced orientation of PA6 crystalline in which the *b*-axis with a negative CLTE orients along the flow direction, and (2) the co-continuous orientation of the rubber and plastic nanolayers, of which the thermal expansion favors towards the normal direction.

1. Introduction

Morphology control plays a crucial role in developing polymer blends with high performance. Generally, the process involves a minor polymer dispersed in another polymer. The blend forms a droplet-continuous (denoted as 0-3 type) structure. If the droplet is subjected to a shear and/or extensional stress, it may be either elongated to a micro-fibril (denoted as quasi 1-3 type) or extended to a microlayer (denoted as quasi 2-3 type), mainly depending on the compatibility and viscoelastic difference between the two polymer melts. Practical applications caused by these morphologies have already been utilized in areas such as super-toughened alloys [1], self-reinforced plastics [2], and gas-barrier products [3]. As the concentration of the minor component increases to a critical value, phase inverse takes place. The droplet domains fuse together and turn into disordered co-continuous (denoted as 3-3 type) structures. Sometimes, they deform into co-continuous microlayers (denoted as 2-3 type) (Fig. 1). In the past decade, much effort has been devoted to polymer blends with co-continuous structures due to their substantial improvements in elastic modulus, heat resistance, and electrical and thermal conductivity [4–7].

Recently, we have discovered that semicrystalline polymer/rubber blends with a 2-3 type structure exhibit a very low coefficient of linear thermal expansion (CLTE) [8]. The reduction of thermal expansion to achieve dimensional stability more comparable with metals is known as one of the major issues for polymers in engineering applications. Traditionally, thermal expansion is suppressed by adding inorganic fillers to the blend [9]. However, because the highly filled composites often suffer from poor toughness, bad appearance as well as difficulty in processing, the reduction in CLTE by this approach remains significantly limited. The blending of elastomers is known to be effective for toughening [1] but tends to worsen the dimensional precision due to its high CLTE. Our preliminary results [8] showed that if rubber domains were deformed into the microlayers and were made co-continuous with the plastic matrix, the CLTE of the polymer blend parallel to the microlayer direction might be reduced to a value even less than that of the highly filled composites. This phenomenon was also observed by Ono et al. [10] and Kim et al. [11] in polypropylene (PP)/elastomer systems. It seems that the morphology control of rubber-toughened plastics may possess substantial potential for designing polymer blends with desirable dimensional stability and impact resistance simultaneously.

The challenge is to fabricate the immiscible plastic/rubber blend co-continuously structured on sub-micrometer scales at a relatively

* Corresponding author. Tel./fax: +86 21 64251661.
E-mail address: wgz@ecust.edu.cn (G. Wu).

0032-3861/$ – see front matter © 2010 Elsevier Ltd. All rights reserved.
doi:10.1016/j.polymer.2010.05.058

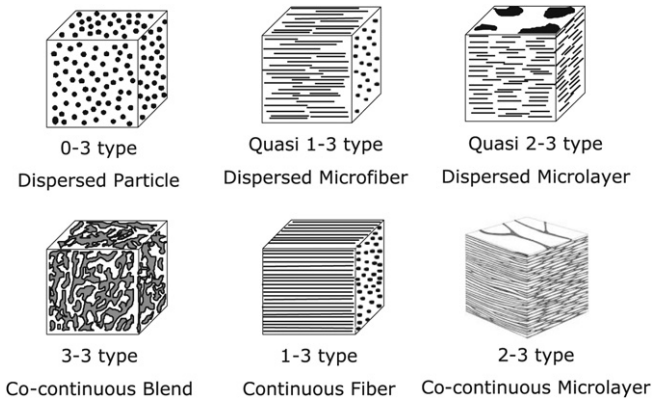

Fig. 1. A schematic diagram of the various morphological types for immiscible polymer blends.

low rubber concentration. A relatively low viscosity of rubber with strong non-linear viscoelasticity should benefit the co-continuous deformation [12]. Another key factor is the compatibility. The addition of compatibilizing agents or compatibilizing agents formed *in situ* helps to control the coalescence and improve the adhesion between the two phases. Pernot et al. [4] reported recently that block copolymers with a molecular polydispersity *in situ* formed by reactive blending of PA6 and polyethylene could broaden the co-continuous window and achieve thermodynamically stable co-continuous nanostructures. Fredrickson et al. [13] also found that ABC ternary block copolymers could enhance the co-continuity of A and C homopolymers. In this work, a triblock elastomer, styrene-ethylene/butylene-styrene (SEBS), grafted with maleic anhydride was used as rubber. The compound PA6 was used as the plastic component. The morphology evolution of the PA6/SEBS blends was traced during the reactive compounding and subsequent injection molding. At a given SEBS loading, a series of phase inversions was observed, transforming the mixture from 3-3 type to 0-3 type and finally to a nanolayer network with a 2-3 type structure.

The mechanism of suppressing the CLTE for plastic/rubber blends with co-continuous microlayer structure is not clear at present. The orientation and crystallization of polymer chains during the injection molding might be the key factors. Thermal expansion of polymers appears to depend largely on the orientation degree of the crystallographic axe along the molecular chain direction [14,15]. Ono et al. [10] confirmed the orientation of PP lamellar crystal in the injection-molded PP/elastomer blend where a negative CLTE of *c*-axis orients parallel to the flow direction. We noticed that crystallization of semicrystalline polymers like PA6 and PP might be confined if the polymer domain is limited within a sub-micrometer space, leading to a transformation of crystalline form and a decrease of both crystallization temperature and crystallinity [16–18]. In order to clarify the influence of morphology on PA6 crystallization and the effects of confined crystallization, crystal orientation and morphology evolution on thermal expansion of the PA6/SEBS blends, a systematical study on the multi-scale orientations (polymer chain, crystal lamellae, and rubber domain), and the confinement of crystallization was carried out in this paper.

2. Experimental section

2.1. Raw materials and sample preparation

The SEBS triblock elastomer used was Kraton G 1901X (supplied by Kraton Polymer), and it had been grafted with 1.84 wt% maleic anhydride and had a molecular weight of 20,000 with a styrene content of 28 wt%. The PA6 (MC161) was supplied by Kanebo with a molecular weight of 65,000. The viscosity measured at a shear rate of 50 rad/s and a temperature of 280 °C for SEBS, and PA6 was 1700 Pa s and 23,000 Pa s, respectively.

These raw materials were dried overnight in an 80 °C oven before blending. They were compounded using a twin-screw extruder (TEX30-2 with a diameter of 30 mm, Nippon Seikosho) at a setting temperature of 250 °C with a screw speed of 200 rpm and a feed rate of 10 kg/h. The mixtures were then subjected to injection molding (IS-90B Model, Toshiba Kikai Seisakusho) at a cylinder temperature of 280 °C under an injection pressure of 80 MPa to prepare 120 × 130 × 3 mm thick sheets. In order to check the morphology evolution of PA6/SEBS (60/40) polymer alloy during the reactive blending, sampling from different positions along the extruding screw was performed. These specimens were compression molded at 280 °C for 10 min under a pressure of 20 MPa. All the samples were placed in vacuum desiccators immediately after molding for 4–6 days at 23 °C prior to the thermal expansion measurements.

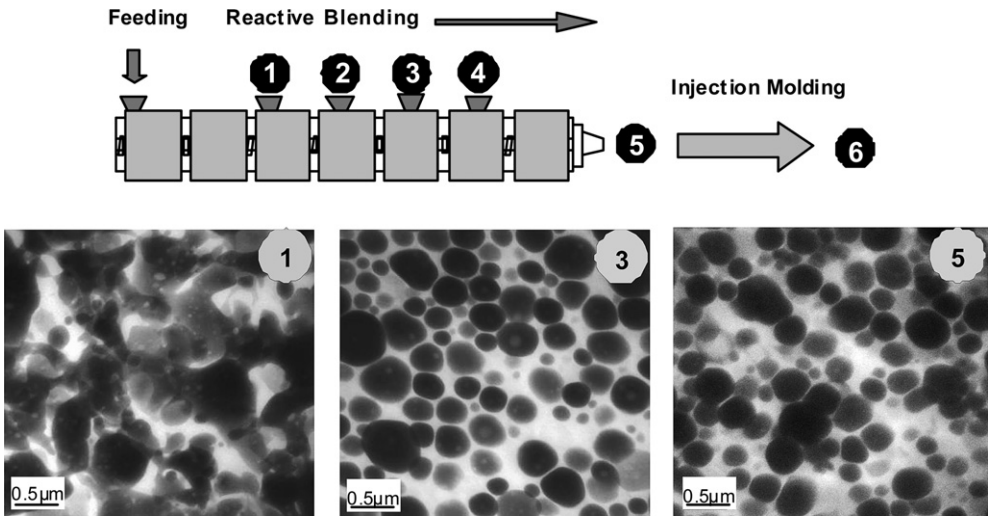

Fig. 2. TEM images of PA6/SEBS (60/40) at different sampling positions along the direction of reactive extrusion as charted above. Dark portions stained by phosphotungstic acid represent the PA6 domains.

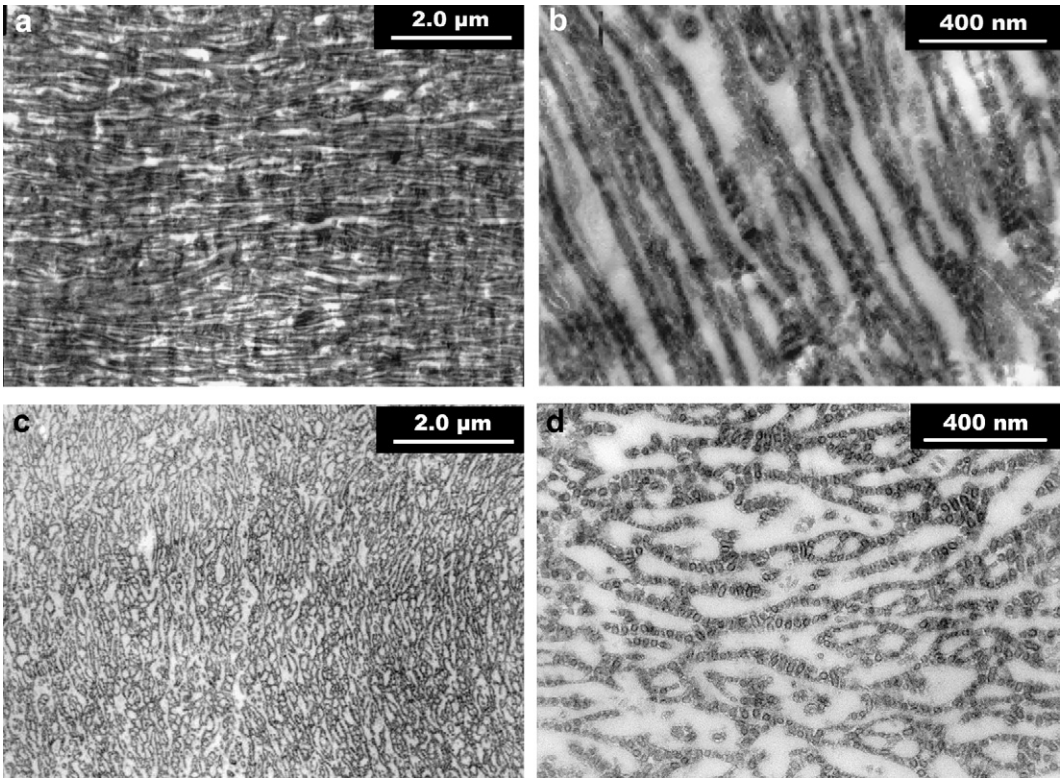

Fig. 3. TEM micrographs of the injection-molded PA6/SEBS (60/40) blend. (a) and (b) were taken in the flow direction and (c) and (d) in the transverse direction. (b) and (d) are the magnified versions of (a) and (c), respectively. The PS domains stained by RuO_4 and OsO_4 vapor in SEBS appear dark.

2.2. Thermal expansion measurements

The CLTE was measured at a heating rate of 2 °C/min using a thermomechanical analyzer (TMA943, Du Pont). To eliminate thermal history and residual stress, the injection-molded and hot-pressed sheets were annealed at 120 °C for 2 h before the test. They were then cut into rectangular specimens by milling the center part of the annealed sheets to the following dimensions: 3 mm in thickness, 5 mm in width, and 6 mm in height. An average value of CLTE from 20 °C to 80 °C was calculated.

2.3. Electron microscopy

Injection-molded samples for TEM analysis were taken from the portion of the surface of the test pieces parallel to the flow direction (FD) and transverse to the flow direction (TD), respectively. They were stained with RuO_4 and OsO_4 vapor at 40 °C for 1 h and were cut into an ultra-thin section approximately 70 nm in thickness using an ultra-microtome (Ultracut N, Reicherr). Hot-pressed specimens were stained with phosphotungstic acid. TEM observation was carried out under a Jeol transmission electron microscope (JEM100CX, Nihon Denshi) at an accelerating voltage of 100 kV.

2.4. X-ray diffraction

Samples for CLTE tests were further used for measuring PA6 crystalline structures by means of a wide angle X-ray diffractor (WAXD) (D/MAX 2550 VB/PC, Rigaku) equipped with a variable temperature attachment. The radiation source employed was CuK α with a wavelength of 0.154 nm scanning at a speed of 8°/min. The 2D diffraction patterns in flow direction (FD), transverse direction (TD), and normal direction (ND) of injection-molded PA6/SEBS were detected by a D8 Discover diffractometer (German Bruker). The corresponding crystal orientation for the *a*-, *b*-, and *c*-axis were calculated according to Herman's orientation function [19,20].

2.5. Differential scanning calorimetry (DSC)

The melting and crystallization behaviors of PA6 and its blends were studied using DSC (TA Q100). Specimens weighing 5–10 mg were moved into the furnace by a robot hand to ensure uniform contact with the thermocouple for each specimen. Before testing, a baseline with both furnaces empty was drawn. Temperature and enthalpy calibrations were performed with indium (Tm = 156.6 °C) and polyethylene oxide (PEO). For the dynamic measurements, the samples were first heated to 260 °C at a rate of 10 °C/min and were kept there for 5 min to erase all thermal history. The samples were

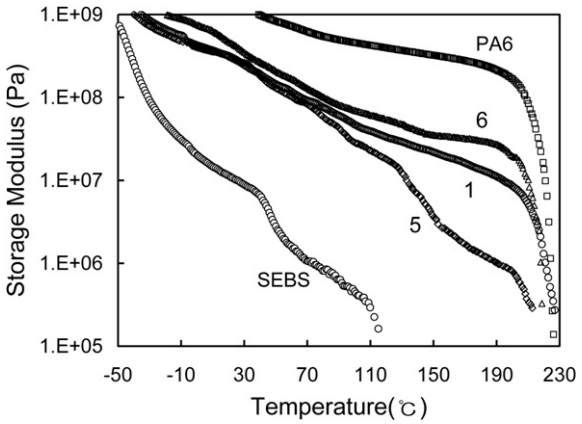

Fig. 4. DMA curves of SEBS, PA6, and their blend (60/40) sampling from Positions 1, 5, and 6.

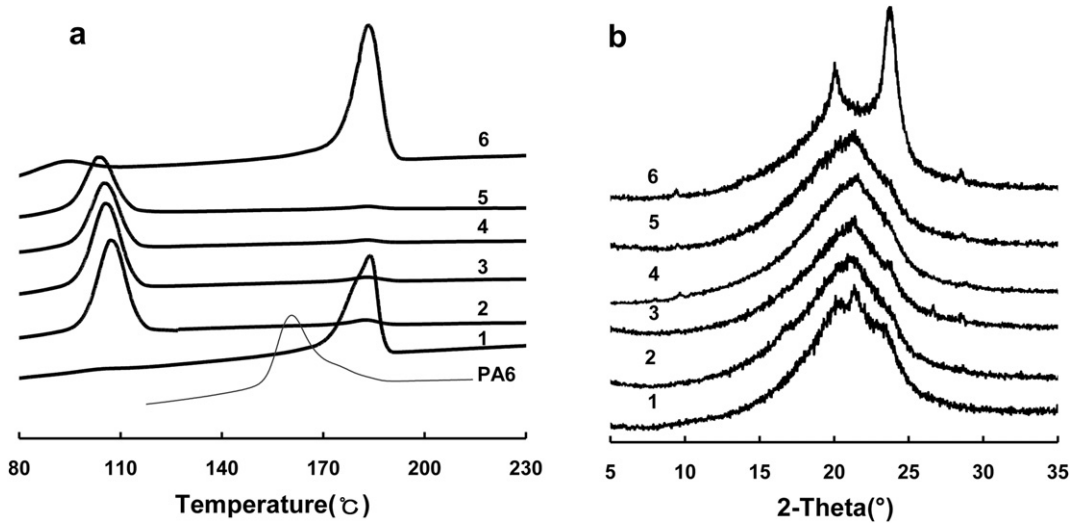

Fig. 5. (a) DSC cooling curves and (b) WAXD profiles for PA6/SEBS (60/40) blend sampling from Positions 1 to 6.

then cooled to −15 °C. Subsequent melting was performed at the same rate. The crystallinity was defined by the ratio of ΔH_c to the heat of fusion of the pure crystalline forms of PA6 (190 J/g) [17,21].

3. Results and discussion

3.1. Morphology evolution of PA6/SEBS (60/40)

Fig. 2 shows the morphology evolution of PA6/SEBS blends along the length of the extruder with a SEBS content of 40 wt%. In the corresponding TEM pictures, the PA6 domains have been stained by phosphotungstic acid and show as dark areas. At sampling position 1, PA6 and SEBS exhibit a co-continuous 3-3 type structure. This could have resulted from a balance between high concentrations of PA6 (60 wt%) and low viscosities of SEBS (the viscosity of SEBS was much lower than that of PA6 as mentioned in Section 2.1). Generally, the co-continuity of a melt-processed binary blend is governed by the composition, viscosity, and compatibility between the two components. A lower critical concentration of SEBS is required for co-continuity due to its much lower viscosity. As the reaction between the maleic anhydride group of SEBS and the amine end group of PA6 continues, *in situ* compatibilizing prevents domain coalescence, leading to a phase transition from the 3-3 type (Position 1) to the droplet-continuous 0-3 type structure (Positions 3 and 5), where the PA6 phase is dispersed in the SEBS matrix with a domain size ranging from 200 nm to 500 nm.

Fig. 3 shows TEM micrographs of the injection-molded PA6/SEBS (60/40) alloy, in which (a) and (b) were taken in the FD and (c) and (d) in the TD. The dark areas in the pictures represent the PS domains in SEBS as stained with RuO_4 and OsO_4 vapor. It is obvious that the SEBS and PA6 phases are elongated and orientated along the FD (Fig. 3a), and are co-continuous (Fig. 3b). Fig. 3c and d shows the morphologies of SEBS and PA6 phases, respectively, transverse to the FD. Again, we observed elongated, orientated, and co-continuous networks with a characteristic thickness of about 20 nm. These pictures clearly illustrate that the 0-3 structured pellets (Position 5) were strongly deformed into a sheet with a co-continuous nanolayer network of 2-3 type structures during the injection molding process.

The morphology changes were further confirmed by dynamic mechanical analysis (DMA) (Rheogel-E-4000, UBM, at a heating rate of 5 °C/min). Fig. 4 shows the storage modulus of PA6, SEBS, and their blend (60/40) sampling from Positions 1, 5, and 6. It is obvious that the storage modulus of the polymer blends is lower than that of neat PA6 but higher than neat SEBS over the entire temperature range. For specimen samplings from Position 5, the storage modulus decreased remarkably at temperatures higher than 110 °C, a temperature corresponding to the melting of the SEBS phase. This suggests that PA6 domains are separated in the SEBS matrix [22]. For Specimens 1 and 6, no abrupt reduction of the storage modulus was observed up to a temperature near the melting point of PA6 (220 °C). Again, this demonstrates the bulk co-continuity of PA6 and SEBS phases. The highest storage modulus among these polymer blends strongly suggests that the co-continuous nanolayer structure forms throughout the injection-molded specimen.

3.2. Crystallization of PA6/SEBS (60/40)

Fig. 5a presents the DSC cooling curves of neat PA6 and PA6/SEBS (60/40) blend sampling from Positions 1 to 6. Table 1 lists the crystallization temperature and heat fusion of these curves. The crystallization temperature increased from 161 °C for neat PA6 to about 188 °C for the specimen 1, indicating the heterogeneous nucleation effect of SEBS on PA6 crystallization [23]. From Specimen 2 to 5, the crystallization peak at 188–190 °C disappeared gradually, and the main crystallization temperature decreased to about 114 °C. We observed that in the injection-molded specimens (at Position 6), PA6 crystallized mostly at a bulk crystallization temperature (190 °C), although it appeared as small peaks at about 107 °C. This result is consistent with previous reports [18] demonstrating that co-continuous morphology can greatly alleviate the confined crystallization.

Table 1
Crystallization temperature and heat fusion of PA6 and PA6/SEBS (60/40) blends sampling from different positions according to DSC cooling curves.

Sampling position	Low-temperature peak		High-temperature peak	
	Tc (°C)	Heat fusion (J/g)	Tc (°C)	Heat fusion (J/g)
Neat PA6			160.78	47.10
1	103.60	1.05	187.95	32.18
2	115.53	24.28	189.41	1.17
3	114.08	23.19	190.98	1.16
4	113.67	23.80	189.29	0.72
5	112.36	23.74	190.52	1.07
6	107.57	4.27	189.93	27.69

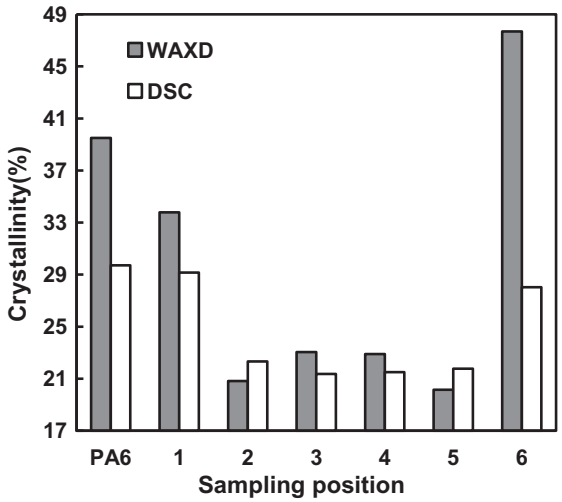

Fig. 6. Crystallinity calculated from the DSC crystallization enthalpy and deconvolution of WAXD curves at different sampling positions.

Changes in the crystallization temperature can account for the transformation of the PA6 crystalline form. Fig. 5b represents WAXD profiles of the PA6/SEBS (60/40) blend from Positions 1 to 6 measured at room temperature. Note that the α crystalline form of PA6 can be distinguished by the location of peak intensities at approximately $2\theta = 20$ and 23.7°, and γ form at 21.3°. Two crystallographic phases, α and γ, can be observed from the WAXD profile for Specimen 1, while for the specimens at Positions 2 to 5, α peak becomes weak and γ peak remains strong. Two diffraction peaks at $2\theta = 20$°and 23.5°are significant for the injection-molded Specimen 6, indicating that the injection-molded PA6/SEBS blend mainly takes on α crystalline.

Many have reported that PA6 exhibits confined crystallization when its droplet size is reduced to a sub-micrometer scale, marked by a transformation of crystalline form from monoclinic α to pseudohexagonal γ and a decrease of both crystallization temperature and crystallinity [16–18]. Combining the above DSC, WAXD, and TEM results, the significant decrease of crystallization temperature for specimens sampling from Positions 2 to 5 should correspond to the morphology change from 3-3 type (at Position 1) to 0-3 type structure where the confined crystallization of PA6 takes place. A slight decrease of crystallization temperature for Specimens 2–5 should be related to a further decrease of the PA6 droplet size along with the reactive blending. The confinement of crystallization is alleviated for the injection-molded specimen, which is in agreement with the co-continuous structure, although the PA6 and SEBS domains are deformed into nanolayer networks.

Fig. 6 shows the PA6 crystallinity calculated from the DSC crystallization enthalpy and WAXD curve deconvolution. The DSC crystallinity was derived from the cooling curves at a non-equilibrium state; thus, a lower value is reasonably compared with that from WAXD. The crystallinity from both the DSC and WAXD was about 20% for specimens with 0-3 type structure (sampling from Positions 2 to 5). For Specimens 1 and 6 with co-continuous structure, PA6 crystallinity increased to a value close to neat PA6. A very high crystallinity (48%) by WAXD was shown by the injection-molded specimen.

3.3. Multi-scale orientation of injection-molded PA6/SEBS

Fig. 7a shows a magnified view of the injection-molded PA6/SEBS (60/40) blend, where PA6 lamella crystal grows perpendicular to the rubber nanolayer. Fig. 7b presents its 2-dimensional X-ray diffraction (2D-WAXD) pattern. The inner and outer circles in the picture represent the (200) and (002/202) crystallographic planes of the PA6 crystal, respectively. These results strongly suggest the existence of PA6 crystal orientation during the rubber and PA6 deformation into nanolayers. According to Herman's orientation function [19,20], the orientation degree of the PA6 crystallographic axe along the FD was estimated to be −0.31, 0.81 and −0.38 for *a*-axis, *b*-axis and *c*-axis, respectively. That is to say, the *b*-axis of the PA6 crystal, which represents the direction of PA6 molecular chains, orients along the flow direction.

TEM observations, together with the 2D-WAXD analysis, reveal that multi-scale orientations take place in the injection-molded PA6/SEBS (60/40) specimen. Firstly, SEBS and PA6 domains deform co-continuously into nanolayer networks along the FD and the TD. Secondly, the PA6 crystal lamellae grow normally along the rubber nanolayers. Thirdly, the *b*-axis of PA6 crystal orients along the flow direction; that is, the molecular chains of PA6 in the crystalline orient parallel with the flow direction. Furthermore, we have confirmed that the *b*-axis of PA6 crystal owns a negative CLTE (-5.8×10^{-5}/°C) [24], which is in agreement to previous reports [25,26]. These multi-scale orientations should contribute to the materials' anisotropic thermal expansion.

3.4. Thermal expansion and molding shrinkage of PA6/SEBS

Fig. 8a shows the influence of morphology evolution on CLTE of PA6/SEBS blends. At a given SEBS content (40 wt%), the CLTE retains the same value for the blends with 3-3 type structure (Position 1) and 0-3 type structure (Position 5); however, it decreases abruptly

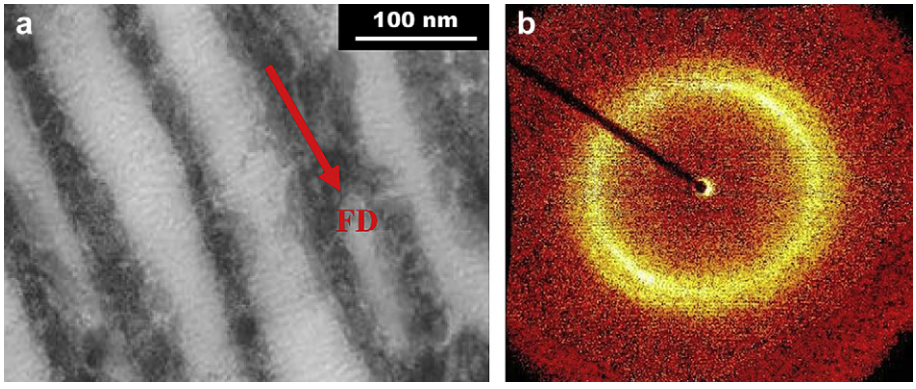

Fig. 7. (a) PA6 crystal orientation observed by TEM micrograph and 2D X-ray diffraction picture.

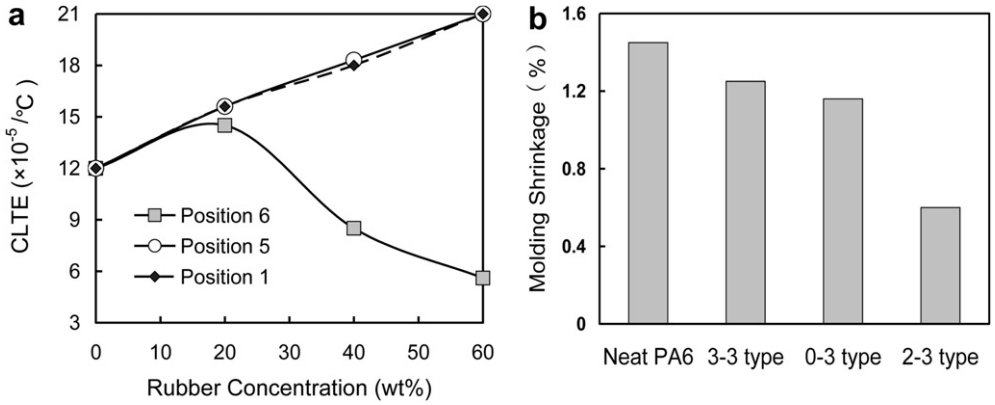

Fig. 8. Influence of morphology on (a) CLTE in the flow direction with different rubber concentrations and (b) molding shrinkage for PA6/SEBS (60/40) blends.

from 18 $\times$ 10^{-5}/°C to 8.0 $\times$ 10^{-5}/°C when the morphology evolves from 0-3 type (Position 5) to 2-3 type (Position 6). Note that the latter value is much lower than that of the injection-molded neat PA6 (12 $\times$ 10^{-5}/°C), although 40 wt% SEBS was added.

The effect of rubber content on CLTE is also presented in Fig. 8a. Similarly, an increase of SEBS content should change morphologies from 0-3 type to 3-3 type and finally to 3-0 type for the reactive blended PA6/SEBS system. A linear increase of CLTE with SEBS content demonstrates clearly that either droplet-continuous structures or randomly co-continuous structures present the same thermal expansion behavior. However, for the injection-molded blends, the CLTE varied greatly with the SEBS content. The CLTE in the flow direction increases when the SEBS content is first increased. When the rubber content surpasses 20 wt%, a drastic reduction of CLTE is observed up to a concentration of 60 wt%. As the rubber domains are deformed into microlayers during the injection molding process, the different tendencies of CLTE variation around 20 wt% SEBS are correlated to the morphology change from a dispersed microlayer to a nanolayer network as verified by TEM observation in Fig. 9.

The morphology evolution also significantly influences the materials' shrinkage during cooling from the compression-molding or injection molding. It is well known that polymers with a lower degree of crystallinity usually lead to less shrinkage. However, the results shown in Fig. 8b demonstrate that the injection-molded PA6/SEBS (60/40) with a 2-3 type structure presents much less shrinkage than that of compression-molding counterparts (either with a 0-3 type or with a 3-3 type structure) despite the fact that it shows a higher degree of crystallinity (see Fig. 6) and experiences a stronger shear force.

The reduction of CLTE and molding shrinkage for the injection-molded PA6/SEBS blends may have originated from the orientation of PA6 crystals because the *b*-axis with a negative CLTE orients along the flow direction. If this is true, the bulk CLTE in the flow direction should result from a competition between the rubber expansion and the amount of rubber-induced orientation of PA6 crystals. At a rubber concentration lower than 20 wt%, the SEBS domains are separated from each other (see Fig. 9), and the rubber expansion may play a dominant role, resulting in the increase of CLTE with SEBS content. When the rubber content increases so that the PA6/SEBS blend deforms co-continuously into a nanolayer network, a large amount of PA6 crystals is oriented. As a result, the CLTE decreases. This tendency is in agreement with the results shown in Fig. 8a.

Aside from the contribution of the crystalline orientation, the nanolayer network structure itself might further promote the reduction of CLTE and molding shrinkage [8]. Fig. 10 summarizes the influence of morphology on the thermal expansion of PA6/SEBS blends for the purpose of better illustration. In the case of 0-3 type or 3-3 type structures, the rubber phase is matrix and distribute in an isotropic pattern, resulting in the linear increase of CLTE with rubber content (see Fig. 10a). However, when PA6 and SEBS domains overlap in a layer-to-layer structure (denoted as 2-2 type) (see Fig. 10b), the CLTE parallel to the layer direction (*x*- and *y*-axis directions) reduces to a value close to that of neat PA6. This occurs because Young's modulus of PA6 is about 100–10,000 times higher than that of SEBS within a temperature range from 20 °C to 100 °C (see Fig. 4), and the expansion of the rubber parallel to the layer direction is restricted completely by the PA6 layers. The increase of CLTE at low SEBS concentrations is reasonable because the SEBS

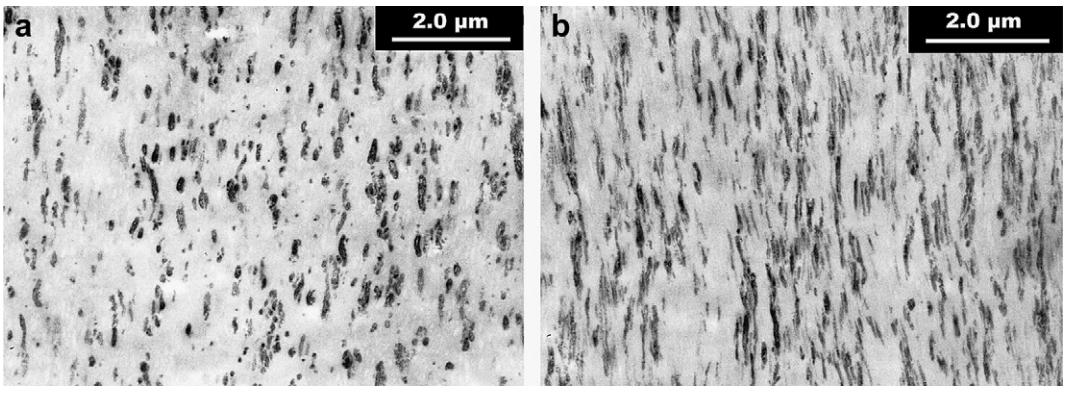

Fig. 9. TEM micrographs of samples from (a) Position 5 and (b) Position 6 for the PA6 blend with 20 wt% SEBS. The PS domains stained by RuO_4 and OsO_4 vapor in SEBS appear dark.

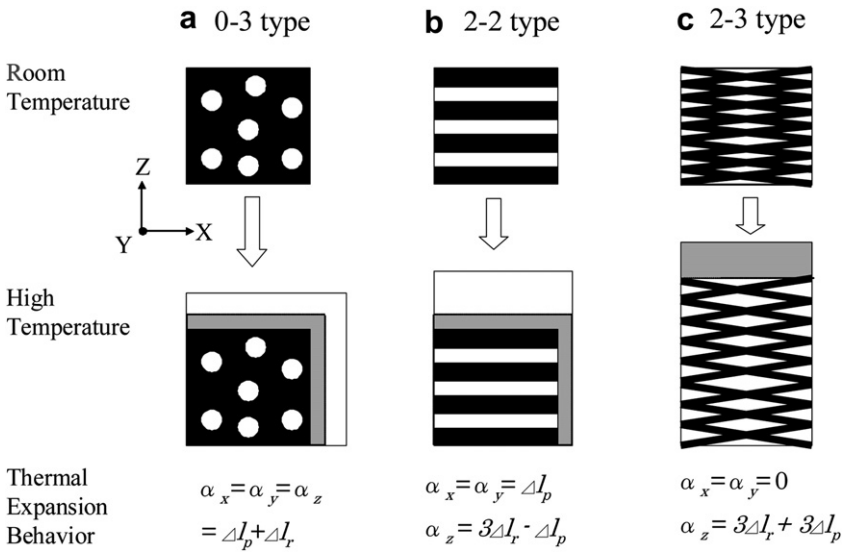

Fig. 10. A schematic diagram of the thermal expansion behavior for plastic/rubber blends with various morphologies. α_x, α_y, and α_z represent the linear thermal expansion in the *x*, *y*, and *z*-axis direction, respectively. Δl_p is the linear expansion per unit from the plastic phase, and Δl_r is from the rubber phase.

microlayers are dispersed in the PA6 matrix, which is not exactly the same as a 2-2 type structure. It should be pointed out that the restriction of rubber expansion by PA6 in the layer direction should not change its bulk expansion volume (as Poisson's ratio of many rubbers is near to 0.5). The rubber has to expand transversely to the layer direction, leading to a high CLTE in the thickness direction (*z*-axis direction).

Further reduction of CLTE in the *x*- and *y*-axis directions may be achieved when the rubber domains are deformed into a nanolayer network (Fig. 10c). Assuming that the aspect ratio of the nanolayer is so high that the thermal expansion of the rubber in the *x*-and *y*-axis directions is highly constrained by the PA6 layers, then, like the thermal expansion behavior of the layer-to-layer structure in Fig. 10b, the rubber layers have to expand towards the thickness direction. In turn, this will suppress the thermal expansion of the plastic in the *x*- and *y*-axis directions because the large volume of the rubber expansion should create a strong force exerted in the thickness direction and draw the three-dimensionally continuous PA6 nanolayers towards the thickness direction. This may be the reason why the CLTE decreases to a value of $5.6 \times 10^{-5}/^{\circ}C$ when the SEBS content is increased up to 60 wt% and why the injection-molded PA6/SEBS (60/40) has very low shrinkage in spite of the high degree of crystallization. We indeed observed a very high CLTE for 2-3 type plastic/rubber blends in the thickness direction [8].

4. Conclusions

The morphology evolution of PA6/SEBS (60/40) from a co-continuous structure to a droplet-continuous structure and finally to a nanolayer network structure during reactive blending and subsequent injection molding was observed and characterized by means of TEM, DMA, DSC, and WAXD measurements. The co-continuous nanolayer structure was achieved due to the high viscosity ratio and *in situ* compatibilizing between the two polymers. The confined crystallization took place only in the blends with a 0-3 type structure where the sub-micrometer sized PA6 particles were dispersed in the SEBS matrix. This led to the transformation of the crystalline form from monoclinic α to pseudohexagonal γ and to a significant decrease of both crystallization temperature and crystallinity. The crystallinity of the injection-molded PA6/SEBS (60/40) blends remained high, although both the PA6 and SEBS domains were critically deformed into nanolayer networks.

It was found that for the injection-molded polymer blends, the PA6 crystal lamellae grew normal in the rubber nanolayers, and the *b*-axis of PA6 crystal oriented along the flow direction. That is, the molecular chains of PA6 in the crystalline oriented parallel with the flow direction. Further, the experiments revealed a negative CLTE of the orientated *b*-axis in PA6 crystal. It was concluded that the large reduction of CLTE and molding shrinkage for the injection-molded PA6/SEBS blends originated from the characteristics of the microstructure in two aspects: (1) the rubber-deformation-induced orientation of PA6 crystalline in which the *b*-axis with a negative CLTE orients along the flow direction; and (2) the anisotropic thermal expansion behavior of the nanolayer network structure. Thus, a plastic/rubber blend with a co-continuous nanolayer network structure is indeed effective in reducing the CLTE in the flow direction due to the preferential expansion towards the thickness direction.

Acknowledgement

This research was supported by grants from the National Natural Science Foundation of China (50873033), Shanghai Pujiang Program (06PJ14028) and Shanghai Leading Academic Discipline Project (B502). The authors also thank Dr. Hironari Sano in Mitsubishi Chemical Corporation, Japan, for the TEM observation (Figs. 3 and 9).

References

[1] Oshinski AJ, Keskkula H, Paul DR. Polymer 1992;33:268–83.
[2] Ke Z, Shi D, Yin J. Macromolecules 2008;41:7264–7.
[3] Cui X, Wang X. J Appl Polym Sci 2006;101:3791–9.
[4] Pernot H, Baumert M, Court F, Leibler L. Nat Mater 2002;1:54–8.
[5] Roy X, Sarazin P, Favis BD. Adv Mater 2006;18:1015–9.
[6] Babinec SJ, Mussell RD, Lundgard RL, Cieslinski R. Adv Mater 2000;12:1823–34.
[7] Gubbels F, Blacher S, Vanlathem E, Jérôme R, Deltour R, Brouers F. Macromolecules 1995;28:1559–66.
[8] Wu G, Nishida K, Takagi K, Sano H, Yui H. Polymer 2004;45:3085–90.
[9] Yoon PJ, Fornes TD, Paul DR. Polymer 2002;43:6727–41.
[10] Ono M, Washiyama J, Nakajima K, Nishi T. Polymer 2005;46:4899–908.
[11] Kim DH, Fasulo PD, Rodgers WR, Paul DR. Polymer 2008;49:2492–506.
[12] Jorgensen JL, Utracki LA. Polymer 2003;44:1661–9.

[13] Fredrickson GH, Bates FS. Eur Phys J B 1998;1:71–6.
[14] Wakelin JH, Sutherland A, Beck LR. J Polym Sci 1960;42:278–80.
[15] Choy CL, Chen FC, Ong EL. Polymer 1985;26:884–8.
[16] Loo YL, Register RA, Ryan AJ, Dee GT. Macromolecules 2001;34:8968–77.
[17] Wu QJ, Liu XH, Berglund LA. Macromol Rapid Commun 2001;22:1438–40.
[18] Tol RT, Mathot VBF, Groeninckx G. Polymer 2005;46:369–82.
[19] Wilchinsky W. J Appl Polym Sci 1963;7:923–33.
[20] Kakudo M, Kasai N. X-ray diffraction by polymers. New York: Elsevier; 1972.
[21] Campoy I, Gomez MA, Marco C. Polymer 1998;39:6279–88.
[22] Sanchez MS, Mathot V, Groeninckx G, Bruls W. Polymer 2006;47:5314–22.
[23] Tang B, Ding XJ, Xue HJ, Li HB, Wu HL. Chem Ind Eng Prog 2008;27:595–601.
[24] Zhou T, Wu GZ. Acta Polymerica Sinica 2008;9:893–8.
[25] Itoh T. Jpn J Appl Phys 1976;15(12):2295–306.
[26] Choy CL, Chen FC, Young K. J Polym Sci 1981;19(2):335–52.